Available online at www.sciencedirect.com
ScienceDirect
Journal of Molecular Catalysis A: Chemical 274 (2007) 185–191
JOURNAL OF MOLECULAR CATALYSIS A: CHEMICAL
www.elsevier.com/locate/molcata

# Hydrothermal synthesis and photocatalytic activity of nanocrystalline $TiO_2$ powders in ethanol–water mixed solutions

Guohong Wang *

*Department of Chemistry and Environmental Engineering, Hubei Normal University, Huangshi 435002, Hubei, PR China*

Received 19 April 2007; received in revised form 6 May 2007; accepted 9 May 2007
Available online 16 May 2007

**Abstract**

Bimodal mesoporous nanocrystalline $TiO_2$ powders were synthesized by a hydrothermal method using tetrabutylorthotitanate as precursor in ethanol–water mixed solutions. The as-prepared $TiO_2$ powders were characterized by X-ray diffraction (XRD), transmission electron microscopy (TEM), high-resolution transmission electron microscopy (HRTEM) and $N_2$ adsorption–desorption measurements. The photocatalytic activity of the as-prepared $TiO_2$ powders was evaluated by the photocatalytic degradation of acetone under UV-light irradiation at room temperature in air. The effects of alcohol content on the microstructures and photocatalytic activity of the $TiO_2$ powders were investigated and discussed. The molar ratios of EtOH to $H_2O$ obviously influenced the crystallization, crystallite size, BET specific surface areas and photocatalytic activity of the prepared $TiO_2$ powders. Hydrothermal treatment enhanced the phase transformation of the $TiO_2$ powders from amorphous to anatase and crystallization. It was found that the photocatalytic activity of $TiO_2$ powders prepared at 150–200 °C for 3–24 h in an ethanol–water mixed solution greatly exceeded that of Degussa P25. All $TiO_2$ powders after hydrothermal treatment showed bimodal pore-size distributions in the mesoporous region: one was intra-aggregated pores with maximum pore diameters of ca. 2–8 nm and the other inter-aggregated ones with maximum pore diameters of ca. 41–48 nm.


*Keywords:* $TiO_2$; Mesopores; Bimodal; Hydrothermal method; Photocatalytic activity

## 1. Introduction

The fabrication of semiconductor photocatalysts has attracted intense interest in the past 10 years because of their unusual optical and electric properties and environmental applications such as air purification, water disinfection, hazardous waste remediation, and water purification [1–6]. Among various oxide semiconductor photocatalysts, titania has been proven to be the most suitable for widespread environmental applications for its biological and chemical inertness, strong oxidizing power, cost effectiveness, and long-term stability against photocorrosion and chemical corrosion [1]. Titanium dioxide has three kinds of phase structures, i.e. anatase, rutile and brookite. The photocatalytic activity of titania is phase dependent. Anatase as a metastable phase usually exhibits the most photocatalytic active due to a low recombination rate of photo-generated electrons and holes. On the contrary, the most stable rutile phase is least active or not active at all [7,8]. Many papers [9–14] have reported that the surface properties such as porous structures, specific surface areas, crystallinity, surface state and porosity obviously influence the photocatalytic activity of titania. However, it is very difficult to estimate the exact contribution of each factor on the photocatalytic activity. For example, specific surface areas and crystallinity usually appear to be two conflicting intrinsic properties for titania nanoparticles [8]. Nonetheless, the anatase $TiO_2$ powders with high BET specific surface areas, good crystallization and relative small crystallite size are desirable to improve the photocatalytic activity by creating more possible reactive sites on the surface of photocatalyst. Among various techniques available for the fabrication of $TiO_2$ nanoparticles, the sol–gel technique has been widely employed due to its low cost equipment required, low temperatures and the homogeneous and highly pure products produced. However, the crystallization of

* Tel.: +86 714 6515602; fax: +86 714 6515602.
*E-mail address:* wanggh2003@163.com.

1381-1169/$ – see front matter © 2007 Elsevier B.V. All rights reserved.
doi:10.1016/j.molcata.2007.05.009

titania often takes place at high temperatures (400–600 °C), and is accompanied with high shrinkage or collapse of the mesostructure and is eventually followed by the increase in nanoparticle size and the decrease in specific surface area [15–17]. To prepare highly photoactive nanocrystalline $TiO_2$ powders, a reasonable route would be to reduce the temperature of the phase transformation of amorphous to anatase [14,18,19].

In recent years, hydrothermal synthesis is widely applied for the preparation of various inorganic materials in nanocrystalline state [20]. Hydrothermal technique is a "soft solution chemical processing", which provides a facilitated route to control grain size, particle morphology, microstructures, phase composition and surface chemical properties via adjusting experimental parameters such as temperature, pressure, duration of process and pH value of solution [20–23]. Furthermore, the nature of the reaction media plays a significant role in controlling the size and morphology of titania nanoparticles [24]. Yang and Gao [24] reported the effects of the benzene phase on the nucleation and growth process of $TiO_2$ nanoparticles in the water-immiscible solvent of benzene system via hydrothermal treatment. Andersson et al. [25] reported effects of hydrochloric acid and nitric acid on crystalline structures, pore size distribution and photocatalytic activity of titanium dioxide synthesized using the method of hydrothermal treatment of microemulsions. Zheng et al. [26] reported the influence of the concentration of the aqueous $TiCl_4$ solution, reaction temperatures and times on the phase, morphology, and grain size of the products. In this work, bimodal nanocrystalline mesoporous anatase $TiO_2$ powder photocatalysts were prepared via a hydrothermal method in an EtOH–$H_2O$ mixed solution and their photocatalytic activity was investigated.

## 2. Experimental

### 2.1. Sample preparation

All chemicals used in this study were reagent-grade without further purification. Deionized water was used in the whole experiment. Tetrabutylorthotitanate ($Ti(OC_4H_9)_4$, TBOT) was used as a titanium source. TBOT (13.2 ml) was added dropwise to 130 ml pure water or EtOH–$H_2O$ mixed solution in a 250 ml beaker under continuous stirring for 30 min. The molar ratio of EtOH/$H_2O$ (***R***) was 0, 1 and 3 and labeled as ***R***0, ***R***1 and ***R***3, respectively. Sol samples obtained by hydrolysis reaction were transferred into a Teflon lined stainless steel autoclave. Hydrothermal reactions were conducted at 100–200 °C for 3–24 h, respectively. After hydrothermal reaction, the white precipitates were centrifuged, and then washed with distilled water and alcohol for five times. The washed precipitates were dried in a vacuum oven at 80 °C for 10 h and finally ground to obtain $TiO_2$ samples.

### 2.2. Characterization

The X-ray diffraction (XRD) patterns obtained on an X-ray diffractometer (type HZG41B-PC) using Cu Kα irradiation at a scan rate of 0.05° $2\theta\,s^{-1}$ were used to determine the identity of any phase present and their crystallite size. The accelerating voltage and the applied current were 15 kV and 20 mA, respectively. Crystallite sizes and shapes were observed by transmission electron microscopy (TEM) and high-resolution transmission electron microscopy (HRTEM) (JEOL-2010F at 200 kV). The samples for TEM observation were prepared by dispersing the $TiO_2$ powders in an absolute ethanol solution under ultrasonic irradiation; the dispersion was then dropped on carbon–copper grids. The Brunauer–Emmett–Teller (BET) surface area ($S_{BET}$) of the powders was analyzed by nitrogen adsorption in a Micromeritics ASAP 2020 nitrogen adsorption apparatus (USA). All the samples were degassed at 180 °C prior to nitrogen adsorption measurements. The BET surface area was determined by a multipoint BET method using the adsorption data in the relative pressure ($P/P_0$) range of 0.05–0.3. Desorption isotherm was used to determine the pore size distribution via the Barret–Joyner–Halender (BJH) method, assuming a cylindrical pore modal [27–29]. The nitrogen adsorption volume at the relative pressure ($P/P_0$) of 0.995 was used to determine the pore volume and average pore size.

### 2.3. Measurement of photocatalytic activity

Acetone ($CH_3COCH_3$) is a common chemical that is used extensively in a variety of industrial and domestic applications. Therefore, we chose it as a model contaminate chemical. Photocatalytic oxidation of acetone is based on the following reaction [30–33]:

$$CH_3COCH_3 + 4O_2 \rightarrow 3CO_2 + 3H_2O \quad (1)$$

The photocatalytic activity experiments on the as-prepared $TiO_2$ powders and Degussa P-25 (P25) were performed at ambient temperature in a 15 l reactor using the photocatalytic degradation of acetone in air with an initial concentration of $400 \pm 20$ ppm. The detailed experimental setup and process have been reported elsewhere [11]. The weight of the $TiO_2$ catalysts used for each experiment was kept at 0.3 g. The acetone vapor was allowed to reach adsorption–desorption equilibrium with catalysts in the reactor prior to UV light irradiation. A 15 W UV lamp with a primary wavelength at 365 nm provided illumination and its intensity striking on the coating measured with a UV radiometer (Model: UV-A, made in Photoelectric Instrument Factory of Beijing Normal University) was $2.9 \pm 0.1$ mW/cm$^2$. The concentration analysis of acetone, carbon dioxide, and water vapor in the reaction was conducted on line with a Photoacoustic IR Multigas Monitor (INNOVA Air Tech Instruments Model 1312). Each set of experiment was followed for 60 min. The photocatalytic activity of the $TiO_2$ samples can be quantitatively evaluated by comparing the apparent reaction rate constants. The photocatalytic oxidation of acetone is a pseudo-first-order reaction and its kinetics may be expressed as follows: $\ln(C_0/C) = kt$ [11], where $k$ is the apparent reaction rate constant, $C_0$ and $C$ are the initial concentration and the reaction concentration of acetone, respectively.

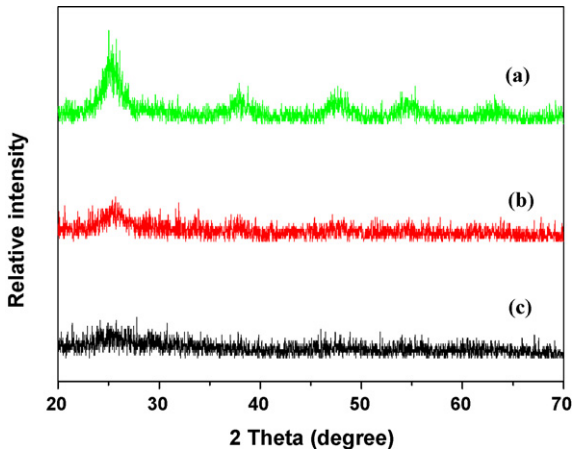


Fig. 1. XRD patterns of the ***R***0 (a), ***R***1 (b) and ***R***3 (c) $TiO_2$ powders prepared at 100 °C for 3 h.

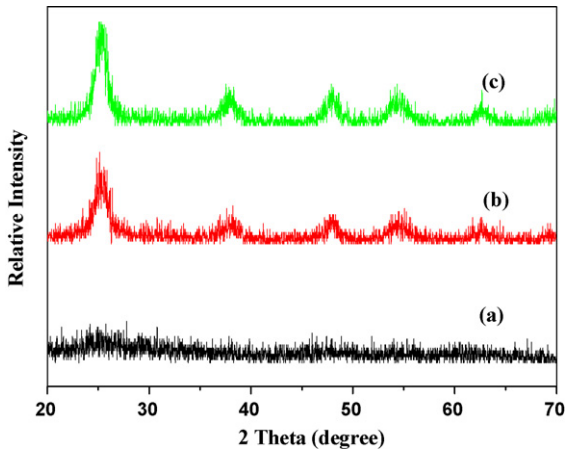


Fig. 2. XRD patterns of the ***R***3 $TiO_2$ powders prepared at 100 °C (a), 150 °C (b), and 180 °C (c) for 3 h.

## 3. Results and discussions

### 3.1. Crystal structure

Fig. 1 shows XRD patterns of the as-prepared $TiO_2$ powders prepared by a hydrothermal method at 100 °C for 3 h from ethanol–water mixed solutions with different ethanol concentrations. The crystal size and relative anatase crystallinity of $TiO_2$ samples are shown in Table 1. It can be seen from Fig. 1 that the $TiO_2$ powders obtained from pure water (***R***0) contain anatase phase. With increasing ***R*** from 0 to 3, the intensities of anatase peaks decrease and the width of the (1 0 1) plane diffraction peak of anatase ($2\theta = 25.4°$) become wider. Further observation shows that the powders appear amorphous at ***R*** = 3. When the TBOT is hydrolyzed at a higher ethanol concentration in the EtOH/$H_2O$ mixed solutions, the rate of hydrolysis reaction is relative low and the hydrolysis is not complete, there are a large amount of un-hydrolyzed alkyls still remaining in the $TiO_2$ powders. These un-hydrolyzed alkyls prevented the phase transformation of amorphous to anatase by adsorbing alkyls on the surfaces of $TiO_2$ particles [14,30]. Consequently, the as-prepared $TiO_2$ powders were amorphous at ***R*** = 3. It can be concluded that the concentration of ethanol in the reaction medium plays an important role in the nucleation, growth and phase transformation of $TiO_2$ nanoparticles during hydrothermal treatment. Usually, with increasing water content, a stronger nucleophilic substitution reaction between $H_2O$ and alkoxide molecules will occur and more alkoxyl groups in the alkoxide will be substituted by hydroxyl groups of $H_2O$ [34]. Therefore, the decrease of the quantity of un-hydrolyzed alkyls in precursors results in reduction in steric hindrance by the residual alkyls preventing crystallization to crystalline anatase [35].

Fig. 2 shows XRD patterns of $TiO_2$ powders prepared from ***R***3 mixed solution after hydrothermally treated at 100 (a), 150 (b) and 180 °C (c) for 3 h. It can be seen from Fig. 2(a) that the $TiO_2$ sample prepared at 100 °C is amorphous. On the contrary, the $TiO_2$ samples after hydrothermal treatment at 150 (b) and 180 °C (c) for 3 h appear anatase phase. Usually, the phase transformation temperature from amorphous to anatase of $TiO_2$ is higher than 400 °C during the calcination. Hence, it can be concluded that hydrothermal treatment enhances the phase transformation of the $TiO_2$ powders from amorphous to anatase at a low temperature. Further observation shows that with increasing hydrothermal temperatures, the peak intensities of anatase steadily become stronger and the width of the diffraction peak of anatase slightly becomes narrower, indicating the formation of greater $TiO_2$ crystallites and the enhancement of crystallization of $TiO_2$. The crystallinity of $TiO_2$ nanoparticles was quantitatively evaluated by comparing the relative intensity of the (1 0 1) diffraction peak of the anatase. Table 1 lists the average crystalline sizes and relative anatase crystallinity of $TiO_2$ samples prepared at different hydrothermal temperatures. It can be seen that the average crystalline sizes and relative anatase crystallinity increase with increasing hydrothermal temperatures.

Fig. 3 shows the effects of hydrothermal time on phase structures of $TiO_2$ powders prepared from ***R***3 mixed solution at

Table 1
Effects of hydrothermal temperatures, time and ***R*** on phase structures and average crystallite sizes of $TiO_2$ powders[a,b]

| ***R***[c] | 100 °C for 3 h | 150 °C for 3 h | 180 °C for 3 h | 180 °C for 10 h | 180 °C for 24 h |
|---|---|---|---|---|---|
| 0 | A:5.3 (1.00) | A:6.8 (1.63) | A:7.1 (1.73) | A:9.1 (1.98) | A:9.4 (2.24) |
| 1 | A:5.0 (0.56) | A:6.4 (1.44) | A:6.9 (1.52) | A:8.8 (1.84) | A:9.3 (1.92) |
| 3 | Am | A:6.1 (1.11) | A:6.8 (1.46) | A:8.6 (1.70) | A:9.1 (1.90) |

[a] Am and A denote amorphous and anatase, respectively.
[b] Average crystalline size of $TiO_2$ was determined by XRD using Scherrer equation. Relative anatase crystallinity: the relative intensity of the diffraction peak from the anatase (1 0 1) plane (indicated in parentheses, reference = ***R***0 sample hydrothermal-treated at 100 °C for 3 h in pure water).
[c] The molar ratios of EtOH/$H_2O$.

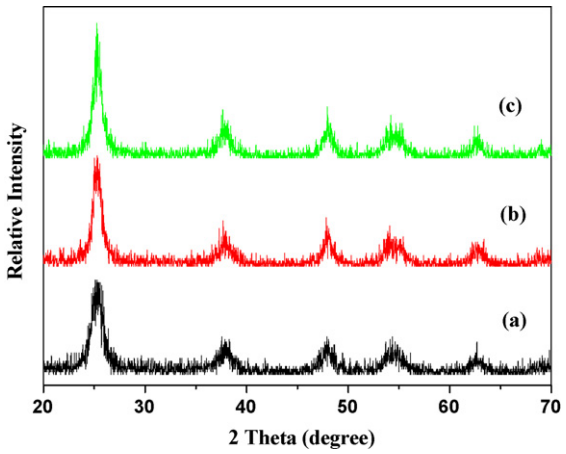


Fig. 3. XRD patterns of the ***R***3 $TiO_2$ powders prepared at 180 °C for 3 h (a), 10 h (b) and 24 h (c).

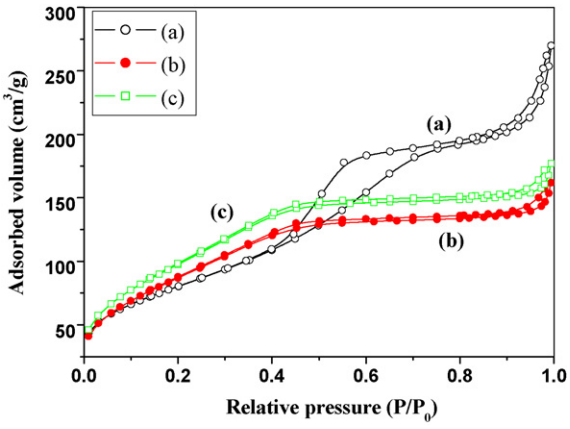


Fig. 5. Nitrogen adsorption–desorption isotherms of the $TiO_2$ powders prepared at initial EtOH/$H_2O$ molar ratios of ***R***0 (a), ***R***1 (b) and ***R***3 (c) and hydrothermally treated at 100 °C for 3 h.

180 °C. It can be seen that with increasing hydrothermal time, the peak intensities of anatase increase and the width of the (1 0 1) plane diffraction peak of anatase ($2\theta = 25.4°$) become narrower.

Table 1 lists the average crystalline sizes and relative anatase crystallinity of $TiO_2$ samples via hydrothermal treatment. With increasing hydrothermal time, the average crystalline sizes and relative anatase crystallinity increase. The appearance of larger particles at longer hydrothermal time suggests that longer hydrothermal times enhance grain growth via a dissolution-reprecipitation mechanism (i.e. Ostwald ripening) in which larger particles grow at expense of smaller ones [36–38].

Fig. 4(a) and (b) shows TEM and HRTEM photographs of $TiO_2$ powders prepared at 180 °C for 10 h at $\boldsymbol{R} = 3$. It can be observed that the primary particles are relative uniform and the sizes of the primary particles are about $9 \pm 2$ nm, which is in agreement with the value (8.6 nm) determined by XRD analysis (see Table 1). Further observation indicates that some of the particles are fused or aggregated together during hydrothermal treatment, which resulting in formation of mesoporous structures. The corresponding HRTEM image of the same sample (Fig. 4(b)) shows clear lattice fringes, which allows for the identification of crystallographic spacing and indicates the prepared anatase $TiO_2$ powders were well crystalline. The fringes of 0.35 nm match that of the (1 0 1) crystallographic plane of anatase $TiO_2$.

### 3.2. BET surface areas and pore distributions

Fig. 5 shows nitrogen adsorption–desorption isotherms of the $TiO_2$ powders prepared at 100 °C for 3 h at initial EtOH/$H_2O$ molar ratios ***R***0 (a), ***R***1 (b) and ***R***3 (c). It can be seen from Fig. 5(a) that the isotherm corresponding to the ***R***0 powders is of type IV (BDDT classification) and have two hysteresis loops, indicating bimodal pore size distributions in the mesoporous region. The shapes of the two hysteresis loops are different from each other. At low relative pressure between 0.4 and 0.7, the hysteresis loops are of type H2, which can be observed in the pores with narrow necks and wider bodies (ink-bottle pores). However, at high relative pressure between 0.8 and 1.0, the shape of the hysteresis loops is of type H3 associated with aggregates of platelike particles giving rise to slit like pores [14,27,39–41]. On the other hand, for the ***R***1 and ***R***3 powders, the isotherms of the $TiO_2$ powders are a combination of types I and IV (BDDT classification) with three very distinct regions: at low relative pressures below 0.2, the isotherm exhibits a high adsorption, indicating that the powders contain micropores (type I). At middle relative pressure between 0.3 and 0.6, small hysteresis loops

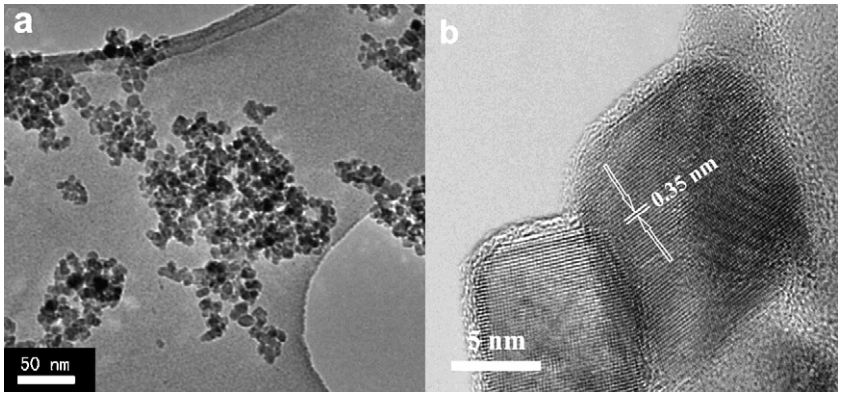


Fig. 4. TEM (a) and HRTEM (b) images of the ***R***3 $TiO_2$ powders prepared at 180 °C for 10 h.

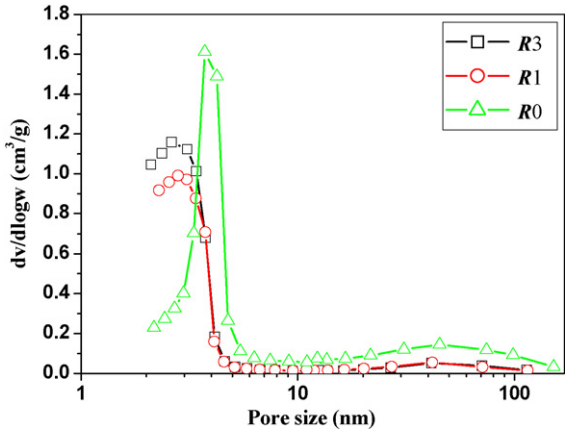


Fig. 6. Pore size distribution of $TiO_2$ powders prepared at different initial EtOH/$H_2O$ molar ratios and hydrothermally treated at 100 °C for 3 h.

are observed and are of type H2, indicating that the samples containing mesopores with narrow necks and wider bodies (ink-bottle pores). At high relative pressures between 0.8 and 1.0, the curve exhibits a small hysteresis loop indicating the presence of larger mesopores (type IV) [27,28].

Fig. 6 shows the corresponding pore size distributions of the ***R***0, ***R***1 and ***R***3 powders after hydrothermal treatment at 100 °C for 3 h. All powders show bimodal pore size distributions consisting of intra-aggregated pores with maximums pore diameters from 2.6 to 3.7 nm and inter-aggregated pores with maximum pore diameters of ca. 41–48 nm. According to the results of Kumar et al. [39], the bimodal pore size distribution arose from the hard aggregated in the powders. In addition, they also reported that there are two types of pores on the bimodal pore size distribution. One is the fine intra-aggregated pore (represented by the hysteresis loop in the lower $P/P_0$ range) and the other is the larger inter-aggregated pore (hysteresis loop in the higher $P/P_0$ range). Furthermore, the micropores in the samples come from amorphous phase [40].

It is interesting to see that the maximum pore sizes of the intra-aggregated and inter-aggregated pores in the ***R***0 powders are larger than those in the ***R***1 and ***R***3 powders. Further observation also shows that with decreasing EtOH/$H_2O$ molar ratios (from ***R***3 to ***R***0), the maximum pore sizes of the intra-aggregated pores shift into larger mesopores regions (from 2.6 to 3.7 nm). This is due to the grain growth from the phase transformation of amorphous to anatase, resulting in the slight increase of pores size (as shown in Tables 1 and 2).

Fig. 7(a)–(c) shows the effects of hydrothermal temperatures on pore size distributions of the ***R***3, ***R***1 and ***R***0 powders prepared at different temperature for 3 h. For the ***R***3 powders obtained at 100–180 °C, the pores show bimodal pore distributions consisting of the intra- and inter-aggregated pores. The maximum pore size of the intra-aggregated pores in the powders prepared at 100 °C lies in 2.6 nm. However, as for the powders prepared at 150 and 180 °C, the maximum pore size of the intra-aggregated pores shifts into larger mesoporous region (ca. 3.8 and 5.2 nm, respectively), indicating the growth of pores. Similar results were also found for the ***R***1 and ***R***0 powders (as shown in Fig. 7(b) and (c), respectively). Therefore, it can be inferred that with

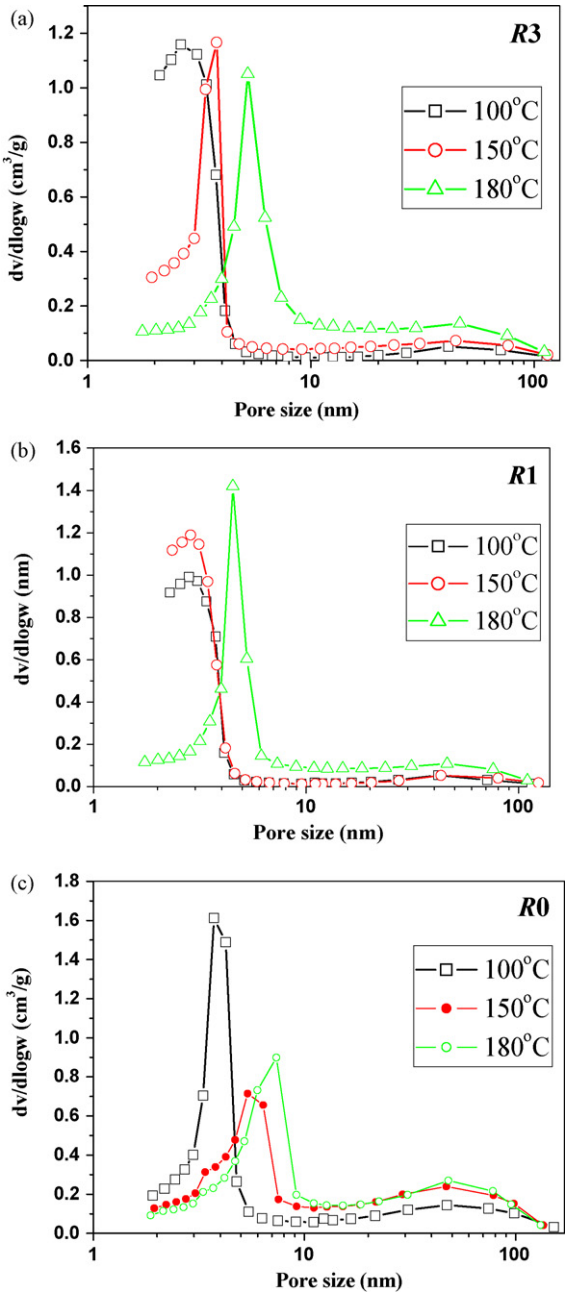


Fig. 7. Pore distribution curves of the ***R***3 (a), ***R***1 (b), and ***R***0 (c) $TiO_2$ powders as a function of hydrothermal temperatures.

increasing hydrothermal temperature the maximum pore sizes of the intra-aggregated pores shift into larger mesopore regions.

Table 1 shows the phase structure and average crystallite size of $TiO_2$ at different hydrothermal temperature, time and ***R***. On one hand, the average crystallinite size and relative anatase crystallinity increase with increasing hydrothermal temperature and time at the same ethanol concentration. This suggests that longer time and higher temperature facilitate crystallization and grain growth of anatase. On the other hand, the relative anatase crystallinity and the average crystallinite size decrease with increasing the ethanol concentration at the same hydrothermal temperature and time. That is ascribed to the fact that lower ethanol concentration in ethanol–water mixed solutions

Table 2
Effects of hydrothermal time and ***R*** on BET surface areas and pore parameters of $TiO_2$ powders prepared at 180 °C

| ***R***[a] | Hydrothermal time (h) | $S_{BET}$ ($m^2/g$)[b] | Pore volume ($cm^3/g$)[c] | Average pore size (nm)[d] | Porosity (%)[e] |
|---|---|---|---|---|---|
| 0 | 3 | 203.8 | 0.378 | 7.4 | 59.5 |
| 1 | 3 | 218.6 | 0.396 | 6.8 | 60.3 |
| 3 | 3 | 232.5 | 0.412 | 6.4 | 61.3 |
| 0 | 10 | 185.6 | 0.364 | 7.8 | 58.6 |
| 1 | 10 | 193.9 | 0.376 | 7.6 | 59.1 |
| 3 | 10 | 208.5 | 0.382 | 7.2 | 59.5 |
| 0 | 24 | 160.1 | 0.286 | 8.5 | 52.7 |
| 1 | 24 | 165.6 | 0.313 | 8.2 | 54.6 |
| 3 | 24 | 174.2 | 0.326 | 7.8 | 55.6 |

[a] The molar ratios of $EtOH/H_2O$.
[b] BET surface area calculated from the linear part of the BET plot ($P/P_0 = 0.05–0.3$).
[c] Total pore volume, taken from the volume of $N_2$ adsorbed at $P/P_0 = 0.995$.
[d] Average pore diameter, estimated using the adsorption branch of the isotherm and the BJH formula.
[e] The porosity is estimated from the pore volume determined using the adsorption branch of the $N_2$ isotherm curve at $P/P_0 = 0.995$ single point.

enhanced hydrolysis of precursors, phase transformation from amorphous to anatase and grain growth [36].

Table 2 shows the effects of ethanol concentration on BET surface areas and pore parameters of $TiO_2$ powders at 180 °C for different hydrothermal time. It can be seen from Table 2 that with decreasing the ethanol concentration, all $TiO_2$ powders show an increase in average pore size and a monotonic decrease in the specific surface areas, pore volumes and porosity. The former is due to the enhancement of crystallization in anatase phase and the growth of crystallites. The latter may be attributable to disappearance of some small pores.

### 3.3. Photocatalytic activity

Acetone as a volatile organic compound was used for the probe reactant to examine the photocatalytic oxidation activities of P25 and synthesized $TiO_2$ powders at different hydrothermal conditions. Fig. 8 shows the dependence of the apparent rate constants ($k$, $min^{-1}$) on hydrothermal temperatures and the molar ratios of $EtOH/H_2O$ (***R***). For comparison, the photocatalytic activity of commercial photocatalyst P25 was also tested

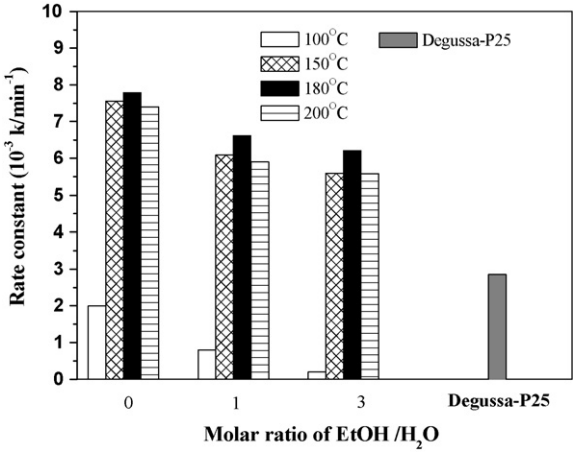


Fig. 8. The dependence of the apparent rate constants ($k$, $min^{-1}$) on hydrothermal temperatures and ***R***, all the samples were hydrothermally prepared for 3 h.

under identical conditions. At ***R*** = 3, for $TiO_2$ powders prepared at 100 °C for 3 h exhibited a very low photocatalytic activity or no photocatalytic activity for the photocatalytic degradation of acetone in air. This is due to the fact that the $TiO_2$ powders are composed of amorphous $TiO_2$ [42,43]. At 150 °C for 3 h, the ***R***3 sample exhibited a decent photocatalytic activity due to the formation of anatase phase [44]. With increasing hydrothermal temperature from 150 to 180 °C, the $k$ increased and reached a maximum value of $6.1 \times 10^{-3}$ at 180 °C. The enhancement of photocatalytic activity at elevated hydrothermal temperatures can be ascribed to an obvious improvement in relative anatase crystallinity (as shown in Table 1) or crystallization (as shown in Fig. 2). The same results are also observed for the ***R***0 and ***R***1 samples. The samples prepared in ethanol–water mixed solutions at above 150 °C for 3 h showed a higher photocatalytic activity than that of P25. The $k$ was determined to be $2.85 \times 10^{-3}$ for Degussa P25 at the same experimental conditions, which is recognized as an excellent photocatalyst [3,45,46]. The superior activity of the prepared $TiO_2$ powders may be ascribed to the following fact that (a) the former has bimodal mesoporous structures, which is more beneficial in enhancing the adsorption and desorption of reactants and products, respectively [47], and (b) the former exhibits larger surface area and smaller crystallite size (as shown in Tables 1 and 2). The specific surface area and crystallite size of P25 are about 53.0 $m^2/g$ and 30 nm, respectively. Large specific surface area allows more gaseous reactants to be absorbed onto the surface of the photocatalyst, while high pore volume allows rapid diffusion of various gaseous products during the photocatalytic reaction, which can enhance the rate of photocatalytic reaction.

Fig. 9 shows the dependence of the apparent rate constants ($k$, $min^{-1}$) on hydrothermal time and the molar ratios of $EtOH/H_2O$ (***R***). It can be seen from Fig. 9 that with increasing hydrothermal time, the $k$ value increases regardless of whether the reaction media is pure water or the $EtOH/H_2O$ mixed solution. The enhancement of photocatalytic activity at longer hydrothermal time can be ascribed to an obvious improvement in relative anatase crystallinity (as shown in Table 1). For example, At ***R*** = 3, for the powders prepared at 180 °C for 10 h, the $k$ reaches the highest value of $7.78 \times 10^{-2}$ due to good crystallization of

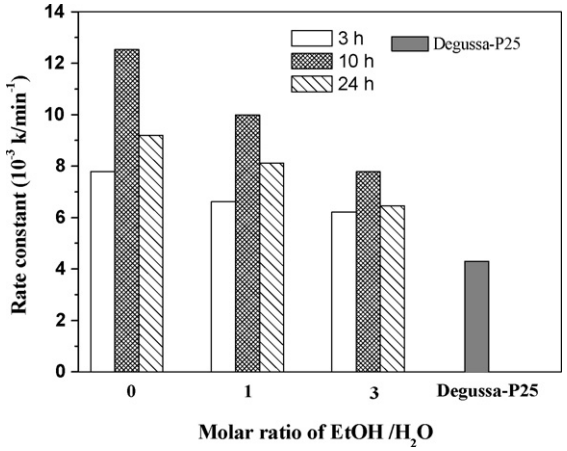


Fig. 9. The dependence of the apparent rate constants ($k$, $min^{-1}$) on hydrothermal time and ***R***, all the samples were hydrothermally prepared at 180 °C.

the samples (as shown in Fig. 4(b)). With further increasing hydrothermal time, the $k$ value decreases probably due to the sharp decrease in BET specific surface areas and increase in crystallinite size (as shown in Tables 1 and 2). The same experimental phenomena are also observed for the ***R***0 and ***R***1 samples. It can also be seen from Figs. 8 and 9 that with an increase in ***R***, the $k$ decreases at the same hydrothermal temperature and time. This is attributed to the fact that the sample prepared at a higher ethanol concentration had weaker crystallization than that prepared at lower ethanol concentration (as shown in Table 1).

## 4. Conclusions

Bimodal mesoporous nanocrystalline $TiO_2$ powders were prepared by hydrolysis of tetrabutylorthotitanate in ethanol–water mixed solutions using a hydrothermal method. Hydrothermal treatment enhanced the phase transformation of the $TiO_2$ powders from amorphous to anatase and crystallization. The molar ratios of EtOH to $H_2O$ obviously influenced the crystallization, crystallite size, BET specific surface areas and photocatalytic activity of the prepared $TiO_2$ powders. All $TiO_2$ powders after hydrothermal treatment showed bimodal pore size distributions in the mesoporous region: one was intra-aggregated pores with maximum pore diameters of ca. 2–8 nm and the other inter-aggregated ones with maximum pore diameters of ca. 41–48 nm. The photocatalytic activity of $TiO_2$ powders prepared at 150–200 °C for 3–24 h showed very high photocatalytic activity and greatly exceeded that of Degussa P25.

## References

[1] M.R. Hoffmann, S.T. Martin, W. Choi, D.W. Bahnemann, Chem. Rev. 95 (1995) 69.
[2] A. Fujishima, T.N. Rao, D.A. Tryk, J. Photochem. Photobiol. C 1 (2000) 1.
[3] A.L. Linsebigler, G. Lu, J.T. Yates Jr., Chem. Rev. 95 (1995) 735.
[4] H. Tada, M. Yamamoto, S. Ito, Langmuir 15 (1999) 3699.
[5] F.B. Li, X.Z. Li, M.F. Hou, Appl. Catal. B 48 (2004) 185.
[6] F.B. Li, X.Z. Li, Appl. Catal. A 228 (2002) 15.
[7] Y.V. Kolen'ko, B.R. Churagulov, M. Kunst, L. Mazerolles, C. Colbeau-Justin, Appl. Catal. B: Environ. 54 (2004) 51.
[8] G. Liu, Z.G. Chen, C.L. Dong, Y.N. Zhao, F. Li, G.Q. Lu, H.M. Cheng, J. Phys. Chem. B 110 (2006) 20823.
[9] J.C. Yu, J. Yu, J. Zhao, Appl. Catal. B 36 (2002) 31.
[10] V. Subramanian, E.E. Wolf, P.V. Kamat, J. Am. Chem. Soc. 126 (2004) 4943.
[11] J.C. Yu, J. Yu, W. Ho, Z. Jiang, L. Zhang, Chem. Mater. 14 (2002) 3808.
[12] B. Ohtani, Y. Ogawa, S. Nishimoto, J. Phys. Chem. B 101 (1997) 3746.
[13] C.P. Sibu, S. Rajesh Kumar, P. Mukundan, K.G.K. Warrier, Chem. Mater. 14 (2002) 2876.
[14] J. Yu, G. Wang, B. Cheng, M. Zhou, Appl. Catal. B 69 (2007) 171.
[15] Q.R. Sheng, Y. Cong, S. Yuan, J.L. Zhang, M. Anpo, Micropor. Mesopor. Mater. 95 (2006) 220.
[16] Z.J. Li, B. Hou, Y. Xu, D. Wo, Y.H. Sun, W. He, F. Deng, J. Solid State Chem. 178 (2005) 1395.
[17] J. Lin, P. Liu, M.J. Meziani, L.F. Allard, Y.P. Sun, J. Am. Chem. Soc. 124 (2002) 11514.
[18] H. Sakai, H. Kawahara, M. Shimazaki, M. Abe, Langmuir 14 (1998) 2208.
[19] G.J. Wilson, G.D. Will, R.L. Frost, S.A. Montgomery, J. Mater. Chem. 12 (2002) 1787.
[20] K. Byrappa, M. Yoshimura, Handbook of Hydrothermal Technology, William Andrew Publishing, New York, 2001.
[21] C. Su, C.M. Tseng, L.F. Chen, B.H. You, B.C. Hsu, S.S. Chen, Thin Solid Films 498 (2006) 259.
[22] G.J. Demazeau, Mater. Chem. 9 (1999) 15.
[23] Y.V. Kolen'ko, V.D. Maximov, A.V. Garshev, P.E. Meskin, N.N. Oleynikov, B.R. Churagulov, Chem. Phys. Lett. 388 (2004) 411.
[24] S.W. Yang, L. Gao, Mater. Chem. Phys. 99 (2006) 437.
[25] M. Andersson, L. Osterlund, S. Ljungstrom, A. Palmqvist, J. Phys. Chem. B 106 (2002) 10674.
[26] Y.Q. Zheng, E.W. Shi, Z.Z. Chen, W.J. Li, X.F. Hu, J. Mater. Chem. 11 (2001) 1547.
[27] K.S.W. Sing, D.H. Everett, R.A.W. Haul, L. Moscou, R.A. Pierotti, J. Rouquerol, T. Siemieniewska, Pure Appl. Chem. 57 (1985) 603.
[28] S.J. Gregg, K.S.W. Sing, Adsorption Surface Area and Porosity, Academic Press, London, 1982.
[29] E.P. Barrett, L.G. Joyner, P.H. Halenda, J. Am. Chem. Soc. 73 (1951) 373.
[30] J. Yu, M. Zhou, B. Cheng, H. Yu, X. Zhao, J. Mol. Catal. A 227 (2005) 75.
[31] J. Lin, J.C. Yu, D. Lo, S.K. Lam, J. Catal. 183 (1999) 368.
[32] M.E. Zorn, D.T. Tompkins, W.A. Zeltner, M.A. Anderson, Appl. Catal. B 23 (1999) 1.
[33] A. Fernandez, G. Lassaletta, V.M. Jimenez, A. Justo, A.R. Gonzalez-Elipe, J.M. Herrmann, H. Tahiri, Y. Ait-Ichou, Appl. Catal. B 7 (1995) 49.
[34] H.F. Yu, S.M. Wang, J. Non-Cryst. Solids 261 (2000) 260.
[35] K. Terabe, K. Kato, H. Miyazaki, S. Yamaguchi, A. Imai, Y. Iguchi, J. Mater. Sci. 29 (1994) 1617.
[36] R.K. Wahi, Y.P. Liu, J.C. Falkner, V.L. Colvin, J. Colloid Interface Sci. 302 (2006) 530.
[37] J.D. Ng, B. Lorber, J. Witz, A. Theobald-Dietrich, D. Kern, R. Giege, J. Cryst. Growth 168 (1996) 50.
[38] R. Boistelle, J.P. Astier, J. Cryst. Growth 90 (1988) 14.
[39] J. Yu, J.C. Yu, W. Ho, M.K.P. Leung, B. Cheng, G. Zhang, X. Zhao, Appl. Catal. A 255 (2003) 309.
[40] J. Yu, H. Guo, S.A. Davis, S. Mann, Adv. Funct. Mater. 16 (2006) 2035.
[41] J. Yu, Y. Su, B. Cheng, M. Zhou, J. Mol. Catal. A 258 (2006) 104.
[42] Y. Sekine, Atmos. Environ. 36 (2002) 5543.
[43] J.G. Yu, H.G. Yu, B. Cheng, X.J. Zhao, J.C. Yu, W.K. Ho, J. Phys. Chem. B 107 (2003) 13871.
[44] H. Yu, J. Yu, B. Cheng, M. Zhou, J. Solid State Chem. 179 (2006) 349.
[45] H. Yu, J. Yu, B. Cheng, J. Mol. Catal. A 253 (2006) 99.
[46] J.C. Yu, J. Yu, W. Ho, L. Zhang, Chem. Commun. (2001) 1942.
[47] J. Yu, J.C. Yu, M.K.P. Leung, W. Ho, B. Cheng, X. Zhao, J. Zhao, J. Catal. 217 (2003) 69.